the debris from the comet itself would have been lost to space after the impact, because most of its vapor plume would have been hot enough to expand at speeds exceeding the escape velocity. For example, to excavate the same-sized crater as the asteroid 100 km in diameter, a comet would need to have a 110-km diameter and travel at 15 km/s, using the equation and assumptions discussed in (*6*), with density $\rho = 1$ g/cm^3. Such an object would produce a total (pulverized + global rock rain) ejecta layer of about 8 m. This is about as thick as the layer for an asteroid (Fig. 1) because most of it originates from the target material.

6. N. H. Sleep, K. Zahnle, *J. Geophys. Res.* **103**, 28529 (1998). We used equation 1 from Sleep and Zahnle and equations 9, 10, 13, and 18 from (*11*) to calculate the volume of debris, from the impactor and target, that escapes, vaporizes, and/or is globally distributed, using 1.4×10^7 J/kg and 6×10^6 J/kg for Qv (energy for complete vaporization) and Qv* (energy for incipient vaporization), respectively. These calculations are velocity-dependent; we have chosen an impacting velocity of 9 km/s.
7. E. Pierazzo, A. Vickery, H. Melosh, *Icarus* **127**, 408 (1997).
8. K. Lodders, B. Fegley Jr., *The Planetary Scientist's Companion* (Oxford Univ. Press, New York, 1998). Types CM and CI carbonaceous chondrites contain 12 to 18% water, respectively.
9. We estimate that the large crater excavates $W_{crater} = 0.25\ \pi\ \phi\ D_{crater}^2\ H$, where we take the porosity of the regolith to decrease exponentially with depth with a scale height, H, of 2.8 km (*29*), and where the porosity at the top of the regolith, ϕ, is 0.2 and the regolith pore space is filled with water.
10. If we presume that thermal radiation from the rock vapor radiates equally up and down, each precipitable centimeter of rock vapor evaporates $\rho_r\ L_{rock}/(2\ \rho_i\ L_{ice}) = 8$ cm of ice (where ρ_r is the density of rock and ρ_i is the density of ice) as the vapor condenses to form molten rock, where $L_{rock} = 1.4 \times 10^{11}$ erg/g is a characteristic latent heat of vaporization for rock. The current martian ice caps cover 1.7% of the planet to an average depth of 1.5 to 2 km (*30*).
11. K. Zahnle, *Spec. Pap. Geol. Soc. Am.* **247**, 271 (1990).
12. We use the correlated-k method to calculate the optical depths for CO_2 and H_2O and a two-stream radiative transfer model to calculate heating rates at each atmospheric level. Eddy diffusion handles vertical transport of static energy, which is used to update temperature and pressure at each level. Surface pressure of CO_2 is assumed to be 150 mbar (*13*). Relative humidity at each level is calculated and as the injected water condenses and rains out, we replace it with a radiatively inert gas to maintain hydrostatic equilibrium. The 30-layer subsurface model solves explicitly for temperature using the diffusion equation. When the temperature in a layer exceeds 273 K, the water melted is calculated and tabulated until that layer is dry. Additional materials and methods are available as supporting material on *Science* Online.
13. D. A. Brain, B. M. Jakosky, *J. Geophys. Res.* **103**, 22689 (1998). Although CO_2 pressures of bars may have occurred on early Mars, Brain and Jakosky have argued that the pressure remaining near the end of heavy bombardment was in the range from 30 to 600 mbar, depending on sputtering and impact erosion. 150 mbar of carbon dioxide only warms Mars a few degrees above its temperature of thermal emission to space, which was about 198 K.
14. W. V. Boynton *et al.* [*Science* **297**, 81 (2002)] used data from the Gamma-Ray Spectrometer onboard the Mars Odyssey to estimate that the current middle- and high-latitude martian regolith may be as much as 35% ($\pm$15%) water by weight, with a 40-cm dry (1% water) cap. We have chosen the lower limit of 20% for our simulations, with a 40-cm (0% water) dry cap to represent global average conditions. We recognize that these numbers pull away from our otherwise conservative approach, because Boynton *et al.* found these numbers to be for the polar regions and not global. However, we note that a colder Noachian Mars probably had a much shallower equatorial ice depth than at present. It is possible that local conditions were much dryer or wetter than these conditions. Runs of our model with a dry (1%) regolith confirm that the water evaporated from the target material and melted in the subsurface (Fig. 4) scales linearly with the water fraction. These two values dominate the curve, so if 1% water, for example, were more correct, the total water precipitated and melted would be 20 times less than our numbers, but there are still plenty of large events in the crater (visible and buried) record to generate the required water for valley formation.
15. M. C. Malin, *Geophys. Res. Lett.* **13**, 444 (1986).
16. Hydrothermal convection will occur in systems when the Rayleigh number, Ra, is greater than 40. The Rayleigh number is given by $Ra = \alpha\rho C_p g\lambda h\Delta T/(\eta k)$ (*31*) where α is the thermal expansion coefficient of water, g is gravity, ρ is the density of water, C_p is the specific heat of water, λ is the permeability of rock, h is the height over which the temperature differences occur, η is the viscosity of water, and k is the thermal conductivity of water. Our impact events have Rayleigh numbers of less than the threshold, so convection is not important. To fully estimate the importance of convection, we would need better information on the porosity of the martian regolith at depth, and so we have not included convection in our model. The most likely scenario for extensive groundwater flow would involve an impermeable capping layer, which would suppress such convection.
17. M. H. Carr, *Water on Mars* (Oxford Univ. Press, New York, 1996).
18. C. B. Leovy, J. C. Armstrong, in preparation.
19. M. H. Carr, M. C. Malin, *Icarus* **146**, 366 (2000).
20. B. M. Jakosky, *Icarus* **55**, 1 (1983).
21. M. P. Golombek, N. T. Bridges, *J. Geophys. Res. Planets* **105**, 1841 (2000).
22. J. B. Pollack, J. Kasting, S. Richardson, K. Poliakoff, *Icarus* **71**, 203 (1987).
23. F. Forget, R. T. Pierrehumbert, *Science* **278**, 1273 (1997).
24. A. Colaprete and O. B. Toon (*J. Geophys. Res.*, in press) found that only 5 to 10 K of warming was achieved when the radiative effects of CO_2 ice clouds were considered, which is not enough to heat the planet above 273 K.
25. R. J. Phillips *et al.*, *Science* **291**, 2587 (2001).
26. J. F. Kasting, *Icarus* **91**, 1 (1991).
27. P. R. Christiansen *et al.*, *Science* **279**, 1692 (1998).
28. M. C. Malin, K. S. Edgett, *Science* **290**, 1927 (2000).
29. The energy supplied by an impactor, added to the energy from the Sun, places Mars into the runaway greenhouse regime of several steady-state models. Given a sufficiently rapid supply of groundwater to the atmosphere, a temporary runaway might have begun. The magnitude of such an event is beyond the scope of this work to determine.
30. D. E. Smith *et al.*, *Science* **284**, 1495 (1999).
31. K. Zahnle, J. Pollack, J. Kasting, *Geochim. Cosmochim. Acta* **54**, 2577 (1990).
32. The authors thank the University of Colorado's Center for Astrobiology (grant NCC2-1052), the NASA Astrobiology Institute through Ames Research Center, and NASA (grant NAG5-6900) for support for this research.

Supporting Online Material
www.sciencemag.org/cgi/content/full/298/5600/1977/DC1
Materials and Methods
Fig. S1
References

3 May 2002; accepted 11 November 2002

Regulation of Oceanic Silicon and Carbon Preservation by Temperature Control on Bacteria

Kay D. Bidle,*† Maura Manganelli,‡ Farooq Azam

We demonstrated in laboratory experiments that temperature control of marine bacteria action on diatoms strongly influences the coupling of biogenic silica and organic carbon preservation. Low temperature intensified the selective regeneration of organic matter by marine bacteria as the silicon:carbon preservation ratio gradually increased from ~1 at 33°C to ~6 at −1.8°C. Temperature control of bacteria-mediated selective preservation of silicon versus carbon should help to interpret and model the variable coupling of silicon and carbon sinking fluxes and the spatial patterns of opal accumulation in oceanic systems with different temperature regimes.

Diatom productivity is largely responsible for downward fluxes of biogenic silica ($BSiO_2$; opal) and organic matter in the global ocean (*1*, *2*). An understanding of the mechanisms that couple the relative fates of diatom Si and C within the water column is critical in order to elucidate the role of diatoms in the biological carbon pump and in order to use opal effectively for paleoproductivity reconstruction.

Oceanic systems display large regional differences in the accumulation and preservation of opal in sediments, but accumulation does not necessarily correspond to C and Si production rates (*3*). Only 25 to 40% of global biogenic silica production occurs above high-accumulation regions (regions consisting of >5% opal by weight), such as coastal upwelling zones, the subarctic Pacific, and the Southern Ocean (*3*, *4*). The Southern Ocean alone supplies ~50% of the global opal accumulation, while accounting for only 20 to 30% of global opal production (*3*–*5*). In contrast, virtually no opal is ac-

Marine Biology Research Division, Scripps Institution of Oceanography, University of California San Diego, La Jolla, CA 92093–0202, USA.

*Present address: Institute of Marine and Coastal Science, Rutgers University, 71 Dudley Road, New Brunswick, NJ 08901–8521, USA.
†To whom correspondence should be addressed. E-mail: bidle@imcs.rutgers.edu
‡Present address: ISPESL–DIPIA, National Institute for Occupational Safety and Prevention, via Fontana Candida, 1, 00040 Monteporzio Catone (RM), Italy.

cumulating below the Sargasso Sea and other oligotrophic midocean gyres, even though their combined annual opal production is also estimated at 20 to 30% of the global average (*3, 4, 6*).

Enhanced preservation of opal is one mechanism that has been proposed to explain high accumulation in open ocean areas, such as the Southern Ocean (*3*). However, recent revisions of the silica budget in the Southern Ocean [giving higher opal production rates (50×10^{12} mol year^{-1} to 80×10^{12} mol year^{-1}) and lower opal accumulation rates (3.1×10^{12} mol year^{-1})] have placed opal preservation efficiencies (the ratio of burial to production) near the global average of 3% (*4, 7, 8*) for the Polar Front Zone (PFZ; 3.1 ± 2.2%), the Permanently Open Ocean Zone (POOZ; 6.3 ± 2.2%), and the Antarctic Circumpolar Current (ACC; 1.2 to 5.5%). Opal sediments in this region now appear to reflect higher annual opal production in surface waters and biogenic opal rain rates than previously thought.

During travel from the surface waters to the sediments, trophic food webs exert differential control over Si and C preservation, resulting in material that is intensely and progressively Si-enriched upon delivery to the seabed (*1, 7, 9*). The strongest increase in the downward Si:C flux ratio (by a factor of 6) is found in the upper water column between the zones of production and export (from 150 to 200 m); the second largest enrichment (by a factor of 4) occurs at the sediment-water interface between the zones of rain and accumulation (*1, 7, 9*). Antarctic siliceous ooze deposits have very high ratios of opal to organic carbon (20 to 60 on a molar basis) (*9, 10*) and display dramatic decoupling in the accumulation of these biogenic phases [opal and particulate organic carbon (POC) are produced in molar ratios of 0.1 to 0.4] (*7, 11*). Continental margin sediments, in contrast, have ratios of opal to organic carbon ~0.6 (as much as 100 times less) and display comparatively tighter coupling (*4*).

Several factors that influence dissolution have been proposed as possible controls of opal preservation: water column depth; opal rain rate; trace element chemistry; aggregation; grazer characteristics; diatom cell morphology (cell size, surface area, and frustule thickness); and temperature (*1, 3, 12, 13*). Temperature is considered to be the main control because the specific dissolution rate (V_{dis}) increases ~10-fold for every temperature increase of 15°C (*14, 15*) and because most opal accumulates in areas with cold surface waters (*4*). Indeed, the lowest V_{dis} values for surface waters have been documented in the ACC (*16*) and the Ross Sea (*17*) (–1.8° to +1.5°C), where accumulation is high. Temperature-dependent differences in Si preservation may also occur throughout the water column, because surface waters experience a wide range of temperatures (–1.8° to >30°C) and most deep ocean waters are consistently cold (~0° to 5°C).

Because seawater is undersaturated with respect to biogenic (amorphous) silica, any exposed raw silica surface undergoes chemical dissolution. Living diatoms protect their silica frustules from dissolution by surrounding them with an organic matrix (*18*). We previously found that bacteria regulate Si regeneration from experimentally lysed diatom detritus (*19, 20*) and from natural diatom blooms in the Monterey, California, upwelling system (*21*) by colonizing and degrading the protective organic matrix surrounding diatom frustules. Bacterial mediation of dissolution suggests that the temperature probably controls not only the chemical depolymerization of silica (*18*) but also the rate of the bacterial removal of the protective organic matrix. The effect of temperature on the two processes is likely sequential and differential; if the removal of the organic matrix were essential for the initiation of silica dissolution, then temperature control would initially be exerted on the rate of degradation of organic matter by the colonizing bacteria. We therefore considered that the temperature control of bacterial action on the organic matrix might influence relative Si and C preservation efficiencies and might contribute to the regional as well as depth-dependent differences in many oceanic systems (*7, 9*).

We compared diatom POC decomposition and $BSiO_2$ dissolution by bacteria isolated from Antarctic waters (–1.8°C) to those isolated from temperate waters off Scripps Pier in La Jolla, California (15° to 20°C) (*22*). We determined whether bacteria mediated different degrees of POC decomposition and $BSiO_2$ dissolution at their respective in situ temperatures (pH 8.0 to 8.2) because of differential temperature regulation of their activities. We also investigated whether wide temperature ranges (from 5° to >30°C), such as those seen vertically through the water column, manifest in temperature-dependent differences between POC decomposition and $BSiO_2$ dissolution by natural bacterial assemblages in California coastal waters. Our experimental system consisted of bacteria acting on axenic uniformly labeled (^{14}C or ^{32}Si) *Thalassiosira weissflogii* detritus of known history (*22*). Parallel incubations in abiotic seawater determined temperature effects on Si and C preservation by chemical processes alone.

Antarctic and California isolates displayed large differences in their abilities to degrade POC and to regenerate $BSiO_2$ at their respective environmental temperatures (Fig. 1A). Antarctic isolates caused strong preferential preservation of Si as compared to C at –1.8°C, because relative POC decomposition was about six times as fast as $BSiO_2$ dissolution. Twenty-one percent (±2%) of diatom POC was regenerated, as compared to 3.5% (±0.9%) of $BSiO_2$ (a V_{dis} of 0.003 to 0.006 day^{-1}) after 7.5 days. Natural diatom assemblages (mostly *Nitzschia* sp.) collected in the Indian sector of the Southern Ocean displayed similarly low V_{dis} (0.002 to 0.004 day^{-1}) when incubating under nonaxenic conditions at comparable pH and temperature (*23*). Substantially higher V_{dis} (0.011 to 0.19 day^{-1}) was obtained, however, for acid-treated frustules of *Thalassiosira* sp. at –1.8°C (*14,*

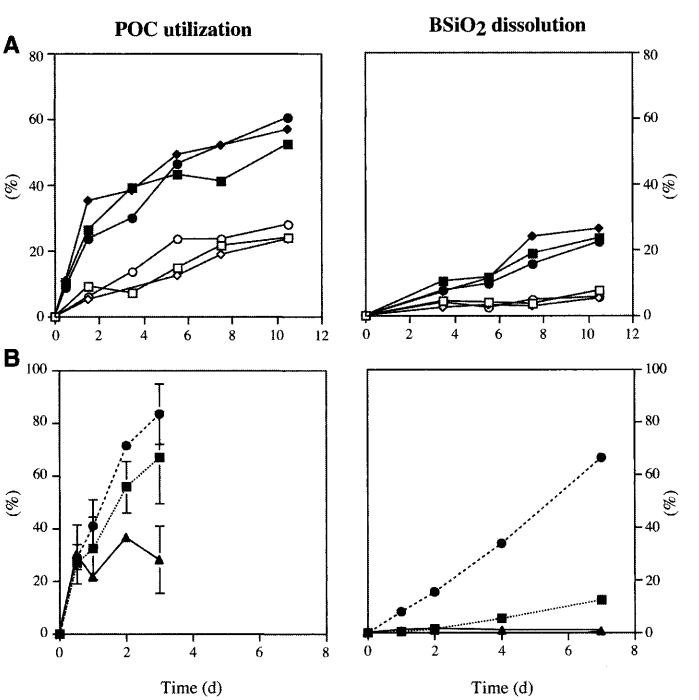

Fig. 1. POC utilization and biogenic silica dissolution for *T. weissflogii* detritus incubating with marine bacteria at various temperatures. (**A**) Marine isolates collected from Antarctic waters (open symbols: squares, PF30-23; diamonds, Ant5-5; circles, Ant5-9) or from Scripps Pier (closed symbols: squares, Tw6; diamonds, Tw7; circles, BBFL7). Incubation temperatures were –1.8 and 17°C for Antarctic and Scripps isolates, respectively. (**B**) A natural bacterial assemblage from Scripps Pier (circles, 33°C; squares, 15°C; triangles, 5°C). Data for detritus incubating in abiotic seawater resembled that from the 5°C incubations.

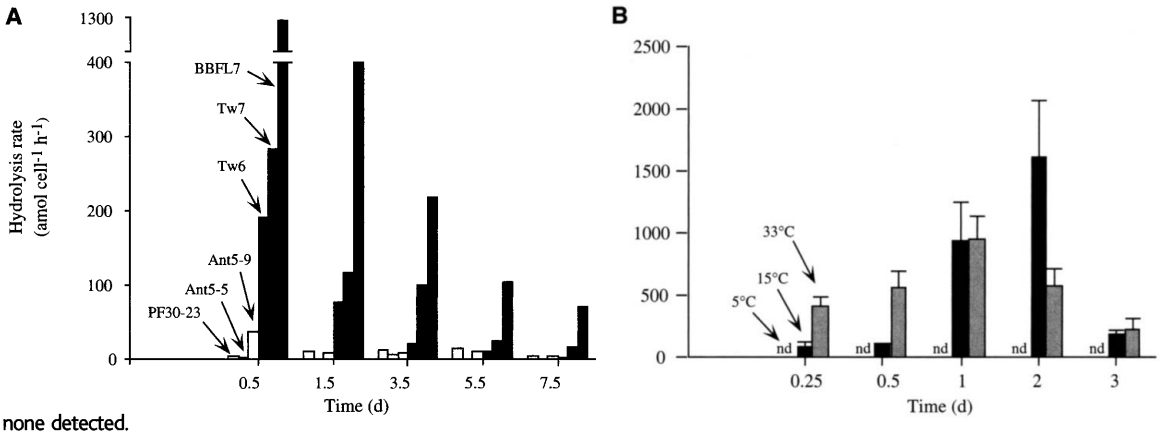

Fig. 2. Cell-specific protease activity of marine bacteria attached to *T. weissflogii* detritus in microcosms incubating at various temperatures. (**A**) Antarctic isolates (open bars) and Scripps Pier isolates (solid bars) incubating at −1.8° and 17°C, respectively. (**B**) Natural bacterial assemblage incubating at 33°, 15°, or 5°C. Activity is expressed as the hydrolysis rate of leucine–amino-4-methylcoamarin. nd, none detected.

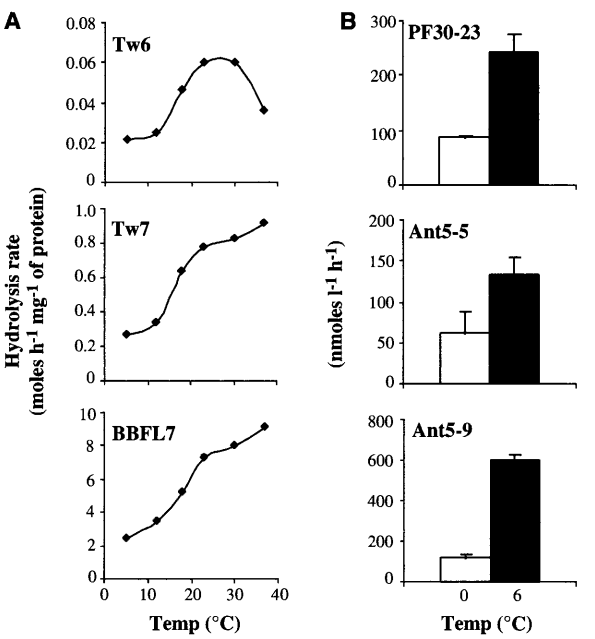

Fig. 3. Temperature regulation of ectoprotease activity. (**A**) Partially purified ectoproteases from temperate Scripps Pier isolates and (**B**) cell-bound ectoproteases from intact Antarctic marine isolates. Equal cell concentrations were used for different temperature incubations in (B).

24), suggesting that temperature regulation of POC degradation considerably influenced Si preservation. Scripps isolates, at 17°C, degraded 50% (±4%) of diatom POC by 7.5 days and mediated higher $BSiO_2$ dissolution (20 ± 4%; V_{dis} of 0.023 to 0.036 day^{-1}), decreasing the Si:C preservation ratio to ~2.4. Kamatani (*15*) found that diatom frustules (collected in net tows and incubated in 0.45-μm-filtered seawater) had a dissolution temperature coefficient (Q_{10}) of 2.27. Our results suggest that this may have been due to temperature regulation of the metabolism of bacteria colonizing diatom frustules (*15*). In our study, V_{dis} displayed a Q_{10} of ~2.3 between −1.8° and 17°C.

Natural assemblages of bacteria also mediated strong temperature-dependent preferential regeneration of C over Si (Fig. 1B). Incubations with *T. weissflogii* at 33°, 15°, and 5°C for 3 days decomposed 83, 66, and 27% of the diatom POC, respectively. Temperature exerted strong control over the bacterial respiration, because 63 and 41% of diatom C was respired in 3 days at 33° and 15°C, respectively (*22*). Only 15% of C was incorporated into bacteria or transferred to the dissolved organic carbon pool at these temperatures. Unexpectedly, bacterial assemblages at 5°C neither measurably respired nor assimilated diatom POC for >3 days, despite large POC enrichment (~60 μM C). Undetectable ectoprotease activity and very low bacterial growth rates (0.02 to 0.4 day^{-1}) indicated that these mesophilic assemblages were physiologically limited at 5°C. For Si, V_{dis} varied by two orders of magnitude (0.001 to 0.138 day^{-1}) between 5° and 33°C with >70% silica turnover at 33°C, after 7 days. *T. weissflogii* detritus silica was very resistant to dissolution under abiotic conditions (V_{dis} 0.001 day^{-1}) at all temperatures (even 33°C), demonstrating the effectiveness of the organic matrix as a protective barrier against chemical hydrolysis. A comparison with the high temperature dependence of organic-free frustules indicated that matrix degradation by bacteria was essential for the initiation of silica dissolution at all temperatures and controlled silica dissolution rates. There was an initial (<12 hours) temperature-independent loss of 20% of POC from frustules in biotic and abiotic incubations, suggesting that some POC was chemically labile but of little consequence to Si regeneration. Based on our results, we predict that the decomposition of diatom detritus and/or aggregates by surface-derived colonizers would be retarded as they sank across the thermocline and would virtually cease at cold depths, with implications for the efficiency of both the biological and silica pumps (*2, 13*).

Bacterial ectoproteolytic hydrolysis of the organic matrix is a key biochemical mechanism regulating silica recycling from diatoms (*19–21*). In this study, warmer temperature hastened and elevated POC hydrolysis by bacteria colonizing diatom detritus and led to earlier initiation of rapid frustule dissolution. The cell-specific protease activities of temperate bacteria were much higher than those of Antarctic bacteria at their respective in situ temperatures (Fig. 2A) (*25–27*). Hydrolysis rates were elevated by as much as three orders of magnitude in the first few days and remained elevated throughout the experimental period (*22*). For temperate natural assemblages, cell-specific proteolytic activities of colonizing bacteria (Fig. 2B) were five times higher at 33°C than at 15°C within 1 day (there was no activity at 5°C) and growth rates were elevated 15- to 30-fold.

The catalytic activity of the ectoproteases of the Antarctic and the temperate bacteria may be temperature–dependent, reflecting their environmental temperature regimes. Responses to temperature among bacterial ectoproteases in subtropical, equatorial, and polar regions (*28*) do suggest distinct bacterial phenotypes with distinct isozymes. In our study, both partially purified ectoproteases from temperate isolates and cell-bound ectoproteases from Antarctic isolates (*22*) had activity optima at higher temperatures than their respective in situ temperatures (Fig. 3). Antarctic isolates were determined to be a mix-

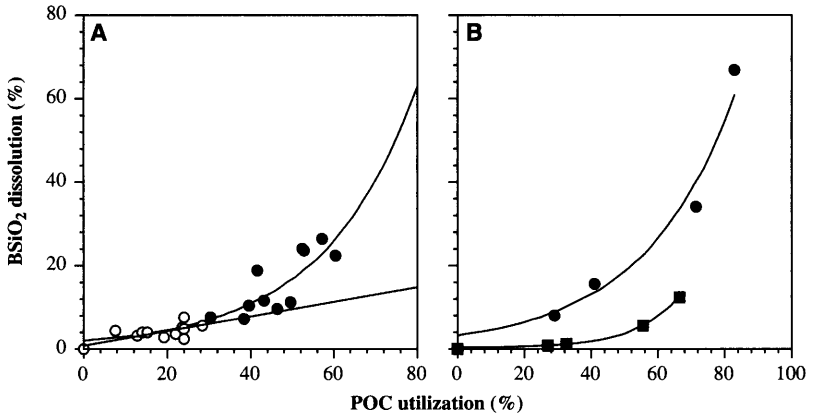

Fig. 4. Relationship between the dissolution of particulate silica and the utilization of POC from *T. weissflogii* detritus incubating with bacteria at different temperatures. **(A)** Antarctic isolates incubating at −1.8°C (open circles) and Scripps isolates incubating at 17°C (closed circles). **(B)** A natural bacterial assemblage incubating at (circles, 33°C; squares, 15°C). Data for solid symbols are fitted to an exponential regression [(A): 17°C: $y = 1.765 \times 10^{0.019x}$, $r = 0.81$; (B) 33°C: $y = 3.016 \times 10^{0.016x}$, $r = 0.99$; 15°C: $y = 0.072 \times 10^{0.034x}$, $r = 0.99$)], whereas data for open symbols are fitted to a linear regression ($y = 0.173x + 0.639$, $r = 0.78$).

ture of psychrotrophs and psychrophiles (*29*), but their growth was strongly inhibited below 0°C. Comparative growth studies between 0° and 6°C showed that Antarctic bacteria were better adapted to cold conditions than were Scripps isolates (fig. S1). Independent field studies evaluating natural microbial assemblages at low ambient temperatures in the Southern Ocean found both psychrophilic (*30*) and psychrotrophic (*28, 31*) responses and found that organic substrate concentration was an important limiting factor (*32*). The relative contribution of psychrophiles and psychrotrophs in permanently cold marine environments remains an open question (*33*) and may influence microbial processing of diatom POC (and associated Si dissolution) in permanently cold oceanic regimes.

An empirical relationship between diatom POC decomposition and $BSiO_2$ dissolution at different temperatures is critical to interpreting their relative preservation dynamics among marine environments with different temperature regimes (*1, 7, 9, 34*). $BSiO_2$: POC fluxes have been measured or modeled for environments ranging from the Southern Ocean to warm oligotrophic gyres (*7, 9*), but they do not differentiate diatom C from other C pools. Here we specifically relate diatom POC decomposition to $BSiO_2$ dissolution for *T. weissflogii* at temperatures from −1.8° to 33°C (Fig. 4), and we demonstrate that the decoupling of C and Si regeneration is highly temperature-dependent. Our results incorporate temperature effects on the chemical dissolution of naked silica frustules (*14, 18*). This functional relationship should retain its general form regardless of diatom identity, although the actual degree of C and Si decoupling may depend on the biochemical makeup and morphology of diatoms. An important feature is that the initiation of rapid $BSiO_2$ dissolution required substantial POC utilization, even at higher temperatures. More extensive C removal was required for silica dissolution at low temperatures, resulting in a progressive increase in the preservation of Si relative to C (from ~1 at 33°C to ~6 at −1.8°C). Slow (but detectable) particulate organic matter hydrolysis and negligible V_{dis} at <0°C led to a larger cumulative POM removal relative to $BSiO_2$. Even a small increase in temperature stimulated POM hydrolysis, presumably exposing a larger surface area of silica frustules to chemical dissolution. Antarctic bacteria at 6°C decomposed 35% (±5%) POC and dissolved 7% (±2%) silica (a V_{dis} of 0.005 to 0.013) after 7.5 days, reducing the Si-to-C preservation ratio to 5 (from 6 at −1.8°C).

Our results provide a mechanistic framework for interpreting observed spatial differences in Si and C preservation in oceanic regions with very different temperature regimes [for example, low molar Si:C flux ratios in the oligotrophic Atlantic (at the BATS site) and very high ratios in the Indian sector of the Southern Ocean (POOZ)] (*9*). Although these differences can be related to dissolved Si availability (*9*), our study demonstrates the important role of temperature regulation in the relative preservation of $BSiO_2$ and POC. Selective stripping of the organic matrix and decoupling of Si and C preservation would be enhanced in permanently cold waters because of inhibition of bacterial activity, combined with slower dissolution of exposed silica. In the ACC, where between 40 and 80% of $BSiO_2$ sinks below 100 m, and where decreases in $BSiO_2$ production (rather than increases in $BSiO_2$ dissolution) explain high $BSiO_2$ dissolution-to-production (D:P) ratios (0.18 to 0.58) (*16*), low surface water temperature may help preserve biogenic silica. However, systems experiencing seasonal temperature shifts may display greater variability in POC and $BSiO_2$ coupling. Extensive recycling of $BSiO_2$ (64 to 82%, and a 40% increase in V_{dis}) in a warm-core ring followed the development of a seasonal nutricline (in the upper 80 m), above which surface water temperatures rose from 16° to 20°C and D:P reached 0.70 (*35*). DeMaster (*4*) has suggested that continental margins replace one-third of silica accumulation attributed to Antarctic deep sea waters, indicating that marine cycles of organic matter and $BSiO_2$ may be coupled more tightly than previously thought.

A better mechanistic understanding of the causal linkages connecting Si cycling, ocean productivity, atmospheric CO_2 levels, and global climate change is critical for predicting the realistic responses of oceanic ecological processes to any future climate change and for calibrating biogenic opal as a paleoproductivity proxy (*36*). Regeneration processes in pelagic waters by trophic food webs lead to the strongest enhancement of Si:C flux ratios and the strongest standard deviation of this enhancement (*9*). At least 95% of organic carbon and 60 to 90% of $BSiO_2$ produced in surface waters return to the dissolved phase in the upper 100 m (*3, 37*). Our study identified bacteria as a critical mechanism of both Si and C diagenesis and further reminds us that temperature is a major variable in Si and C biogeochemistry. Si/C coupling in pelagic waters will depend on factors that couple diatom biomass to the microbial loop (*38*), such as temperature fluctuation (*39*), bacterial species identity and activity (*20, 21*), grazing rates (*13*), and aggregation (*40*), in addition to factors that influence the Si:C content in diatom cells, such as Fe stress (*41*) and Si limitation (*42, 43*). Diagnostic models need to include parameterizations for the effects of bacteria and temperature to help us better understand and constrain the coupling and decoupling of C and Si biogeochemical cycles in the modern ocean.

References and Notes

1. D. M. Nelson, D. J. DeMaster, R. B. Dunbar, J. W. O. Smith, *J. Geophys. Res.* **101**, 18519 (1996).
2. A. R. Longhurst, W. G. Harrison, *Prog. Oceanogr.* **22**, 47 (1989).
3. D. M. Nelson, P. Tréguer, M. A. Brzezinski, A. Leynaert, B. Quéguiner, *Global Biogeochem. Cycles* **9**, 359 (1995).
4. D. J. DeMaster, *Deep-Sea Res. Part II Top. Stud. Oceanogr.* **49**, 3155 (2002).
5. P. Tréguer *et al.*, *Science* **268**, 375 (1995).
6. M. A. Brzezinski, T. A. Villareal, F. Lipschultz, *Mar. Ecol. Prog. Ser.* **167**, 89 (1998).
7. D. M. Nelson *et al.*, *Deep-Sea Res. Part II Top. Stud. Oceanogr.* **49**, 1645 (2002).
8. P. Pondaven *et al.*, *Nature* **405**, 168 (2000).
9. O. Ragueneau, N. Dittert, P. Pondaven, P. Tréguer, L. Corrin, *Deep-Sea Res. Part II Top. Stud. Oceanogr.* **49**, 3127 (2002).
10. D. J. DeMaster, T. M. Nelson, S. L. Harden, C. A. Nittrouer, *Mar. Chem.* **35**, 489 (1991).
11. M. A. Brzezinski, *J. Phycol.* **21**, 347 (1985).

12. D. C. Hurd, S. Birdwhistell, *Am. J. Sci.* **283**, 1 (1983).
13. R. C. Dugdale, F. P. Wilkerson, *Nature* **391**, 270 (1998).
14. A. Kamatani, J. P. Riley, *Mar. Biol.* **55**, 29 (1979).
15. A. Kamatani, *Mar. Biol.* **68**, 91 (1982).
16. D. M. Nelson, L. I. Gordon, *Geochim. Cosmochim. Acta* **46**, 491 (1982).
17. D. M. Nelson, J. A. Ahern, L. J. Herlihy, *Mar. Chem.* **35**, 461 (1991).
18. J. C. Lewin, *Geochim. Geophys. Acta* **21**, 182 (1961).
19. K. D. Bidle, F. Azam, *Nature* **397**, 508 (1999).
20. ———, *Limnol. Oceanogr.* **46**, 1606 (2001).
21. K. D. Bidle, M. A. Brzezinski, R. A. Long, J. Jones, F. Azam, in preparation.
22. Materials and methods are available as supporting material on *Science* Online.
23. P. Tréguer, A. Kamatani, S. Gueneley, B. Quéguiner, *Polar Biol.* **9**, 397 (1989).
24. Dissolution rate constants (per day) at −1.8°C were obtained using dissolution data for acid-treated frustules of *T. decipens* incubating at various temperatures [table 2 in (*14*)]. Data were graphed [the inverse of temperature (in degrees kelvin) versus the natural log of the silica dissolution rate constant (*k*)] and fitted to a linear regression. Ranges in dissolution rates were obtained by graphing data for the first stage ($\ln k = -12789[\text{temp}]^{-1} + 39.423$; $r = 0.94$) and the second stage ($\ln k = -8705.7[\text{temp}]^{-1} + 27.267$; $r = 0.99$) separately. The higher range value of 0.19 day^{-1} represents the first stage of dissolution, when fragile frustule parts dissolve out quickly. The lower range value of 0.11 day^{-1} represents the second stage of dissolution, when hard parts dissolve slowly.
25. The protease activities (2 to 710 nmol liter^{-1} day^{-1}) of Antarctic isolates exposed to diatom detritus in this study accurately represented the dynamic range of protease activities previously observed for natural assemblages in different sectors of the Southern Ocean from 1991 to 1994 (37 to 1200 nmol liter^{-1} day^{-1}).
26. J. R. Christian, D. M. Karl, *Antarct. J. U.S.* **27**, 170 (1992).
27. ———, *Antarct. J. U.S.* **28**, 221 (1993).
28. ———, *Limnol. Oceanogr.* **40**, 1042 (1995).
29. R. Y. Morita, *Bacteriol. Rev.* **39**, 144 (1975).
30. R. E. Hodson *et al.*, *Mar. Biol.* **61**, 89 (1981).
31. R. B. Hanson, D. H. Pope, *Antarct. J. U.S.* **16**, 130 (1981).
32. L. R. Pomeroy, W. J. Wiebe, *Aquat. Microb. Ecol.* **23**, 187 (2001).
33. D. M. Karl, in *Antarctic Microbiology*, E. I. Friedmann, Ed. (Wiley-Liss, New York, 1993), vol. 1, pp. 1–63.
34. D. J. DeMaster *et al.*, *Oceanography* **5**, 146 (1992).
35. M. A. Brzezinski, D. M. Nelson, *Deep-Sea Res.* **36**, 1009 (1989).
36. O. Ragueneau *et al.*, *Global Planet. Change* **26**, 317 (2000).
37. E. Suess, *Nature* **288**, 260 (1980).
38. F. Azam *et al.*, *Mar. Ecol. Prog. Ser.* **10**, 257 (1983).
39. L. R. Pomeroy, D. Deibel, *Science* **233**, 359 (1986).
40. A. L. Alldredge, C. C. Gotschalk, *Deep-Sea Res.* **36**, 159 (1989).
41. S. Takeda, *Nature* **393**, 774 (1998).
42. E. Paasche, *Mar. Biol.* **19**, 117 (1973).
43. M. A. Brzezinski, R. J. Olsen, S. W. Chisholm, *Mar. Ecol. Prog. Ser.* **67**, 83 (1990).

44. We thank M. Brzezinski for discussion and critical reading of the manuscript and two anonymous reviewers for comments. Supported by grants from NSF.

Supporting Online Material

www.sciencemag.org/cgi/content/full/298/5600/1980/DC1

Materials and Methods

Fig. S1

12 July 2002; accepted 31 October 2002

Olmec Origins of Mesoamerican Writing

Mary E. D. Pohl,[1]* Kevin O. Pope,[2] Christopher von Nagy[3]

A cylinder seal and carved greenstone plaque bearing glyphs dating to ~650 B.C. have been uncovered near the Olmec center of La Venta in Tabasco, Mexico. These artifacts, which predate others containing writing, reveal that the key aspects of the Mesoamerican scripts were present in Olmec writing: the combination of pictographic and glyphic elements to represent speech; the use of the sacred 260-day calendar; and the connection between writing, the calendar, and kingship. They imply that Mesoamerican writing originated in the La Venta polity.

Our excavations at San Andrés, located 5 km northeast of the Olmec center of La Venta, produced a cylinder seal and a greenstone plaque with glyphs dating to ~650 B.C., indicating that writing and the calendar originated in the Mexican Gulf Coast region together with other elements central to Mesoamerican civilization. By the Late Formative period (400 B.C. to A.D. 200), three related hieroglyphic scripts and an associated calendrical system had appeared in three different geographic areas (*1*, *2*) (Fig. 1): the Mayan script extending from the Yucatan Peninsula to the Pacific slope of Guatemala and El Salvador, the Isthmian script extending from the Mexican Gulf Coast through the Isthmus of Tehuantepec, and the Oaxacan script of the Valley of Oaxaca, Mexico. These three Late Formative writing and calendrical systems have close similarities, indicating that they probably developed from a common ancestral script (*3*, *4*) during the preceding Middle Formative period (~900 to 400 B.C.).

Before the discovery of glyphs at San Andrés, the earliest examples of writing and calendrics were attributed to Monument 3 from the Valley of Oaxaca site of San José Mogote (*2*). Monument 3 depicts a slain captive with two glyphs inscribed below the body, probably giving the calendrical name of the victim based on his day of birth in the 260-day sacred Calendar Round (Fig. 1). Monument 3 was originally assigned an age of 600 to 500 B.C., but archaeological, iconographic, and linguistic analyses suggest that Monument 3 dates between 300 B.C. and A.D. 200 (*3*, *5*, *6*). San José Mogote Monument 3 would be contemporaneous with similar, Late Formative monuments depicting glyphs associated with defeated capitals and slain captives from the nearby site of Monte Albán.

San Andrés (Fig. 1) was a subsidiary elite Olmec site within La Venta's sociopolitical network, which encompassed a system of dense settlement along the river levees of the Tabascan coastal plain (*7*). La Venta, with its monumental architecture covering 200 ha, was the preeminent center in Mesoamerica during the Middle Formative period, with influence extending from Central Mexico to El Salvador (*8*, *9*). Excavations at San Andrés in 1997 and 1998 (*10*) yielded a rare sample of primary Olmec living debris: floors, hearths, pits, and midden deposits including well-preserved refuse from festival and feasting activities. This refuse contained human and animal bone, oversized beverage preparation and food serving vessels, large hollow figurines, and a ceramic cylinder seal and engraved greenstone plaque fragments yielding evidence of writing and calendrics.

Charcoal from near the base of the stratigraphic unit that contained the seal and greenstone plaque fragments produced a date of 2490 ±40 radiocarbon years before the present (yr B.P.) (Beta-122241), or a calibrated 2σ calendar date of 792 to 409 B.C. (cal B.C.) with an intercept date of 636 cal B.C. (*10*). Charcoal from two strata above the deposit with the seal and plaque fragments produced a date of 2340 ±90 yr B.P. (Beta-112668), or a calibrated 2σ calendar date of 764 to 182 cal B.C. (intercept date of 398 cal B.C.) (*10*). These dates have large calibration error margins because of the nature of the radiocarbon calibration curve during this time period. The dates are supplemented by a ceramic chronology from San Andrés's well-stratified midden deposits. Excavations at San Andrés uncovered two distinct strata containing ceramics assigned to the Early Franco ceramic phase, which spans the period from 700 to 500 cal B.C. The seal, greenstone plaque fragments, and 636 cal B.C. radiocarbon date come from the lower stratum. Thus, the radiocarbon dating and the ceramic chronology both indicate that the seal and greenstone plaque fragments date to approximately 650 cal B.C.

[1]Department of Anthropology, Florida State University, Tallahassee, FL 32306, USA. [2]Geo Eco Arc Research, 16305 St. Mary's Church Road, Aquasco, MD 20608, USA. [3]Department of Anthropology, Tulane University, New Orleans, LA 70118, USA.

*To whom correspondence should be addressed. E-mail: mpohl@mailer.fsu.edu